HIGH PRESSURE VAPOR TRANSPORT OF $ZnGeP_2$: II. THREE-DIMENSIONAL SIMULATION OF GASDYNAMICS UNDER MICROGRAVITY CONDITIONS [1] [2]

J. S. Scroggs, H. T. Banks, K. Ito, S. Ravindran, and H. T. Tran
Center for Research in Scientific Computation
Department of Mathematics
North Carolina State University
Raleigh, NC, USA

and

K.J. Bachmann, H. Castleberry, N. Dietz
Department of Materials Science and Engineering
North Carolina State University
Raleigh, NC, USA

Abstract

The fluid dynamics in a vertical reactor for high pressure vapor transport (HPVT) of compound semiconductors is modeled. The modeling is for the growth of II-IV-V_2 chalcopyrite $ZnGeP_2$ and addresses the flow of dense phosphorus gas at 3.42×10^5 Pascals pressure. Effects of density variations on p-polarized reflectance spectroscopy are also examined. The mathematical model for transport processes is described by the full gasdynamic equations (Navier Stokes equations coupled with an equation for energy). In addition, buoyancy effects are included in the model through the gravitational term in the momentum equation. Numerical results of a 3-D steady flow are presented using a finite element discretization with non-uniform, quadrilateral elements. The numerical simulations were performed to study the effects of gravitational-induced buoyancy-driven convection flows in HPVT crystal growth.

Introduction

Non-linear optical interactions in birefringent materials find applications in phase-matched harmonic generation and frequency mixing. In particular, $ZnGeP_2$, which has a high non-linear susceptibility coefficient, has been used for manu-

[1] This work was supported by National Aeronautics and Space Administration grant #NAGW-2865, and by the National Science Foundation grant #DMS-9201252.

[2] To appear in the proceedings of the International Symposium on Experimental Methods for Microgravity Materials Science, TMS Annual Meeting, February 12-16, 1995, Las Vegas, Nevada

facturing frequency agile infrared lasers and second harmonic generation (SHG) of infrared (CO_2 laser) radiation. Typically, these materials have been processed using bulk crystal growth techniques (solidification); however, there are several shortcomings to this processing method. Namely, residual absorption within its transparency range due to impurities and native defects limits the performance and lowers the laser damage threshold of $ZnGeP_2$ non-linear optical devices that are built with bulk single crystals. Thus in-plane non-linear interactions in high quality heteroepitaxial films become an attractive alternative. In addition, heteroepitaxial structures generally provide for greater beam coherency lengths than achievable with bulk single crystals.

Fluid dynamics limitations to the uniformity of deposition and etching processes have been overcome by operating at low vapor densities. However, some of the most important applications pertain to infrared laser sources which require μm thick films. This mandates epitaxial deposition at rates higher than those which can be achieved at low densities. The associated density gradients in a gravitational field will induce natural convective flows. Convection, in turn, influences the growth processes in two different ways, one of which is beneficial and the other of which is not. Convection increases the overall transport and, thus, the growth rate, which is desirable. On the other hand, it can also affect the morphology of the solid adversely. Thus, we are motivated to study crystal growth under reduced gravity conditions. One potential advantage of such study is that, under low gravity environment, buoyancy-driven convection is reduced (see for example [1]). In particular, a study of this paper is the role of gravitational acceleration and its impact on the thermal and flow fields. Numerical calculations of the isotherms show that temporal gradients are relatively unaffected by the orientation of the ampoule with respect to the gravitational vector and in the microgravity environment ($< 10^{-4}\mathbf{g}$). However, near earth condition temporal variations become more eminent. Successful growth of $ZnGeP_2$ under reduced gravity conditions is greatly enhanced by both development of noninvasive measurement techniques, and by understanding the gasdynamics under which nucleation and growth occurs.

P-polarized reflectance spectroscopy (PRS) is a new non-intrusive method of real-time process monitoring with applicability to vapor deposition and etching processes and contactless temperature measurements. The method has potential to provide for real-time generation of data that characterize materials processing experiments in space. Thus, the success of the experiment can be judged, and, in the case of problems, corrective actions could be implemented from the ground as the experiment progresses.

PRS has been used to monitor the growth of GaP on Si [2]. Fig. shows a schematic representation of PRS. A light beam that is parallel-polarized to

the plane of incidence impinges on the surface at the Brewster angle ϕ_B of the substrate. The changes of the reflectivity as a function of film thickness can be expressed analytically on the basis of the Fresnels equations [3]. Due to interference phenomena, minima and maxima are observed in the time evolution of the reflectivity as the film grows. Detailed information regarding the nucleation and epitaxial overgrowth process was obtained from the analysis of the reflected and scattered radiation. The growth conditions for GaP on Si were, however, low pressure. To extend PRS to higher vapor densities (such as needed for $ZnGeP_2$), it is expected that density variations will have a significant impact on the beam angle through bending (see the section Effect on Beam Angle below). Study of temporal and spatial density variations that might effect the beam path is one of the topics of this study.

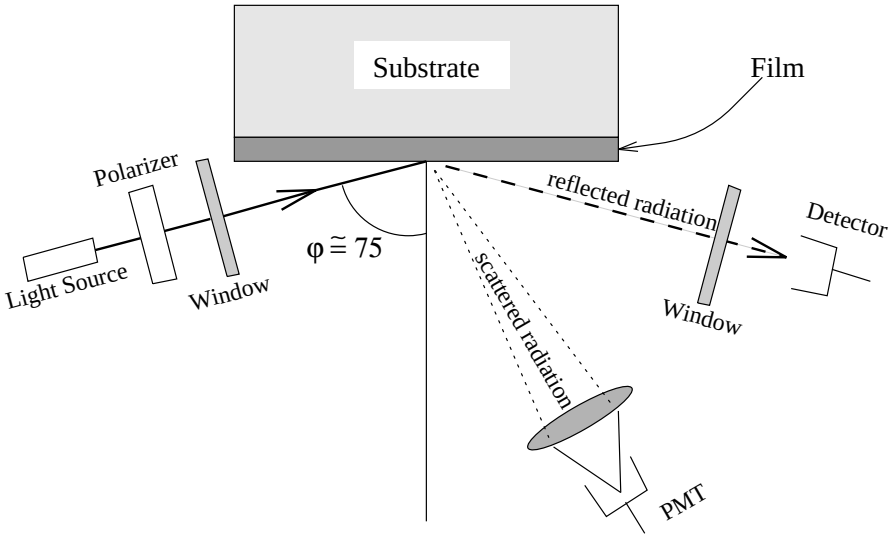

FIG. 1. *Schematic of PRS*

We address the application-driven research to develop mathematical models based on gas-dynamics equations which accurately describe gas flow and deposition processes for HPVT reactors and state-of-the-art computational algorithms to construct optimal control synthesis for regulation of epitaxial deposition process operating at high vapor densities. The first stage in this process is the development of robust and accurate (numerical) simulations of the dominant physical phenomenon governing the fluid dynamics as presented here.

Since 1984 steady progress has been made in the modeling of chemical vapor deposition processes. For example, Moffat and Jensen [4] have used a fully parabolic flow approximation in axial direction for a 3D horizontal reactor. Gokoglu et al. [5] have studied the deposition of Si with a more detailed 3D flow treatment in a similar reactor geometry. In [6], various 2D and 3D models of a horizontal chemical vapor deposition reactor were investigated and the results

were compared with experimental data. This is not the first theoretical study of the effects of gravity on the flow conditions inside a high-pressure vapor transport reactor [7, 8]. Recently, we have completed two-dimensional simulations utilizing a model with multiple species [9]. Studies have also been made concerning the choices that need to be made in the thermal boundary conditions to optimize the vapor transport from the source and to establish uniform flow at the surface of the substrate [10]. In addition to the parameter studies, a more rigorous approach to the optimal design and control has been taken. In [11] the shape optimization problem with respect to the geometry of the reactor and a boundary temperature control problem were formulated. The material and shape derivatives of solutions to the Boussinesq approximation were derived. Optimality conditions and a numerical optimization method based on the augmented Lagrangian method were developed for boundary control of Boussinesq flow. Numerical calculations in [12] indicated the effectiveness of temperature control through a portion of the boundary for improving the vertical transport of flow in the cavity.

The paper is organized as follows. In Mathematical Model, the fluid mechanics associated with thermo-solutal convection is described. A specific HPVT system, boundary conditions, and gas properties used in numerical experiments are introduced in HPVT System and Boundary Conditions. The results of our 3D numerical simulations including some scaling analyses are presented in Simulation Results. In the section Effect on Beam Angle, we study the effect of density/temperature variations on the laser beam used by p-polarized reflectance spectroscopy as an optical in-situ method for layer growth characterization.

Mathematical Model

The mathematical model for the transport phenomena involved in the HPVT process is described by the Navier Stokes equations with an equation for energy. The gas is assumed to be homogenous, thus gas phase reactions and diffusion (Soret and Fickian) are ignored. The evaporation and condensation in the source and substrate regions, respectively, are also ignored. We assume that the flow is laminar and incompressible, and compute the time-averaged solution. Several simplifications have been introduced to make the simulations more tractible. More accurate models would include multiple species thermal (Soret) diffusion of the species since this effect is expected to be significant with the large spatial temperature variations of this experiment (see e.g. [6] and the references given therein). There may also be significant effects from the source and deposition. These two effects, along with gas-phase reactions can have an impact on the simulation, and are planned to be incorporated into the model in the future.

In Cartesian coordinates the steady-state transport can be described by: Conservation of mass:

$$\nabla \cdot \mathbf{u} = 0, \tag{1}$$

Conservation of momentum:

$$\rho_0 \left(\mathbf{u} \cdot \nabla \mathbf{u}\right) = -\nabla P + \mu \nabla^2 \mathbf{u} - \rho_0 \beta \mathbf{g} T, \tag{2}$$

Conservation of energy:

$$\rho_0 c_p \left(\mathbf{u} \cdot \nabla T\right) = \kappa \nabla^2 T. \tag{3}$$

The right-most term in Eqn. (2) repesents the Boussinesq approximation to buoyancy forces [13]. Since the average temperature $\bar{T}$ is large relative to the temperature differences, $\beta = 1/\bar{T}$ is a good approximation to the thermal expansion coefficient. Here, $\mathbf{u} = (u, v, w)^T$ is the vector of unknown velocities in the x, y, and z directions, respectively, and the unknown T represents the absolute temperature. The magnitude and direction of the gravity vector $\mathbf{g}$ will be modified to study reduced-gravity conditions. The system of Eqns. (1)-(3) is called the Bousineseq equations. Density variation is modeled in the gravitational force under the assumption of the perfect gas law

$$P = \frac{\rho R T}{M}, \tag{4}$$

where R is the gas-law constant and M is the molecular weight of the gas. Values for the viscosity μ, the thermal conductivity k, and the specific heat at constant pressure c_p are given below.

HPVT System and Boundary Conditions

A modified Scholz geometry ampoule is expected to be used for the growth experiments of $ZnGeP_2$ (see Figs. 2)-(3).

This is an initial design used to study the qualitative behavior of the gas flow. The source material and the growing crystal are hermetically sealed in fused silica ampoule with three tubes. The larger tube has inner diameter $.028m$ and length $.028m$, and the two smaller quartz tubes have inner diameter $.01m$, and length $.01m$. The smaller tubes are attached to the large tube such that their axis is at an angle of $\phi_B = 75^o$ from the axis of the larger tube, and such that a laser beam has a clear path at the ϕ_B angle to the substrate region. Connected to the center of the ampoule is a fused silica tube, terminating in a flat fused silica window, from which heat can be extracted in a controlled manner by a jet of nitrogen gas

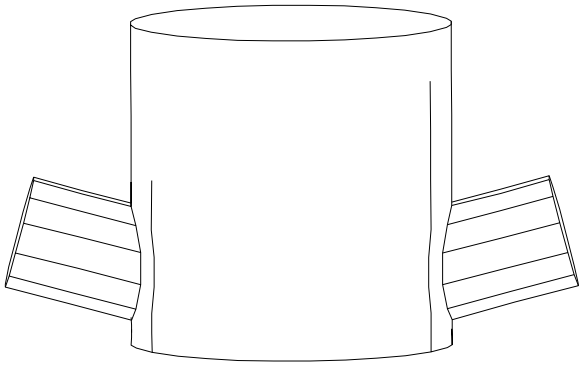

FIG. 2. *Side view of reactor ampoule*

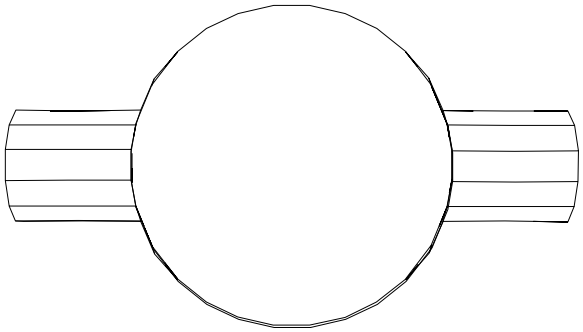

FIG. 3. *Top view of reactor ampoule*

directed onto its outer surface. Due to the lower temperature at this window, the $ZnGeP_2$ transport can be modeled via evaporation from the hot source and condensation on the cooled window.

No-slip boundary conditions are applied to the velocity on all interior surfaces, and $T = 1293^{o}$K except at the top of the chamber which will be cooled with a jet of gas. The temperature on this top surface is $T = 1293 - 15(x^2 + y^2)/r^2$, where $(x, y) = (0, 0)$ is the center axis and $r = .014$ is the radius of the of the larger diameter tube, respectively. The gravity vector is modified for each of the runs, and is described in the next section.

Parameters

A melt of the compounds will be used as the source for vapor phase growth. Heating of $ZnGeP_2$ in an evacuated, closed system causes thermal decomposition of the material, but can be estimated via Gibbs free energy minimization tech-

niques. Using these techniques, the vapor phase composition of $ZnGeP_2$ at the melting point $T = 1295^o$ K has been estimated [14, 15].

From the data in [14], we concluded that the gas phase is dominated by P_4 (and some P_2) gas. Thus we assume a homogeneous gas that is 87.9% P_4 and 12.1% P_2. The physical constants in Table 1 are obtained by weighting the constants for P_2 and P_4 at $T = 1300^o$ K from [16] by these percentages. The reference density ρ_0 was determined from Eqn. 4 using a reference temperature of 1308^oK. It should be noted that in this model the transport properties are constant; however, when there is a large variation in temperature more complicated models for these properties might be needed.

TABLE 1
Gas properties

Property	Value
μ	2.937×10^{-5} m^2/s
k	2.643×10^{-2} J/m $-$ s $-$ K
M	116.3g/l
c_p	654.8 J/kg $-$ K
ρ_0	3.663 kg/m^3

Simulation Results

The coupled gasdynamic equations (1)-(3) were solved numerically with the above mentioned boundary conditions using finite-elements (FIDAP 7.0) with nonuniform, rectangular elements and the pressure correction solver. The computations were performed on IBM, Sun SPARCstation, and Dec workstations with CPU times for a typical simulation being 1-3 hours. We have compared the numerical results of our coarse grids to finer grids and observed negligible variations, an indication that the transport phenomena simulated in the numerical experiments presented here to be well resolved. Simulations were performed with gravity variations from Earth gravity $\mathbf{g}$ to microgravity $10^{-6}\mathbf{g}$, with ampoule orientation as in the figures.

Visualizations of two of the flows at earth gravity $\mathbf{g}$ and $10^{-2}\mathbf{g}$ are shown in Figs. 4 and 5, respectively, with the legend for the isotherms given in Table 2. We choose $10^{-2}\mathbf{g}$ because this is the value of the force where conduction is observed to dominate convection as a heat transport mechanism. These figures show velocity vectors and isotherms from a cut of the flow taken across the middle of the ampoule in a plane perpendicular to the windows. As seen from Table 3, the maximum speed for flows is proportional to the magnitude of the gravity

simulated. The data in Table 3 does not vary in magnitude (the exponential factor does not change) with ampoule orientation.

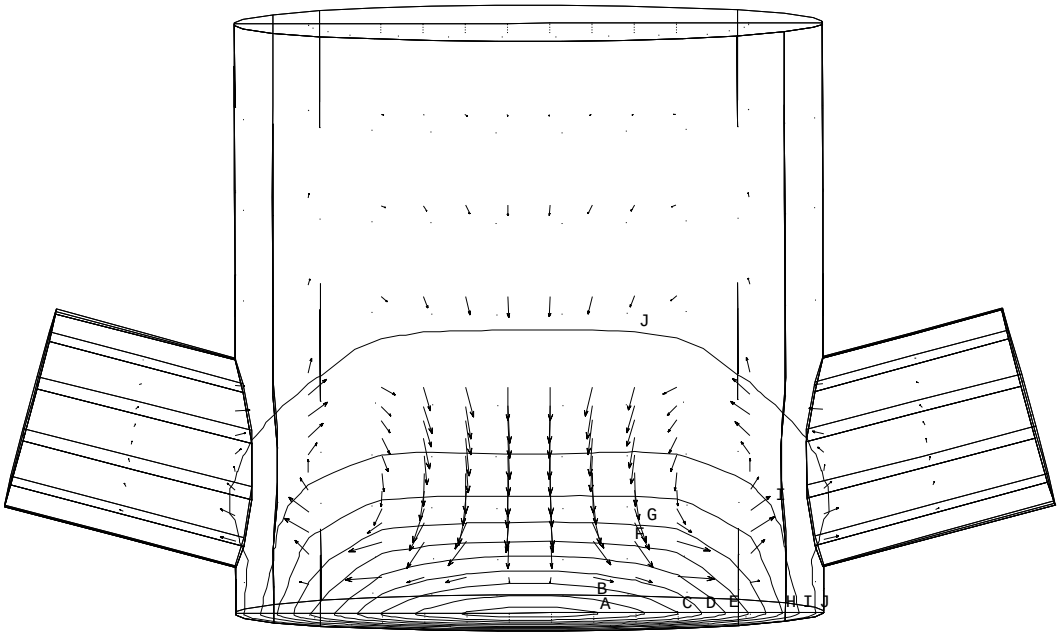

FIG. 4. *Velocity vectors and isotherms at Earth gravity*

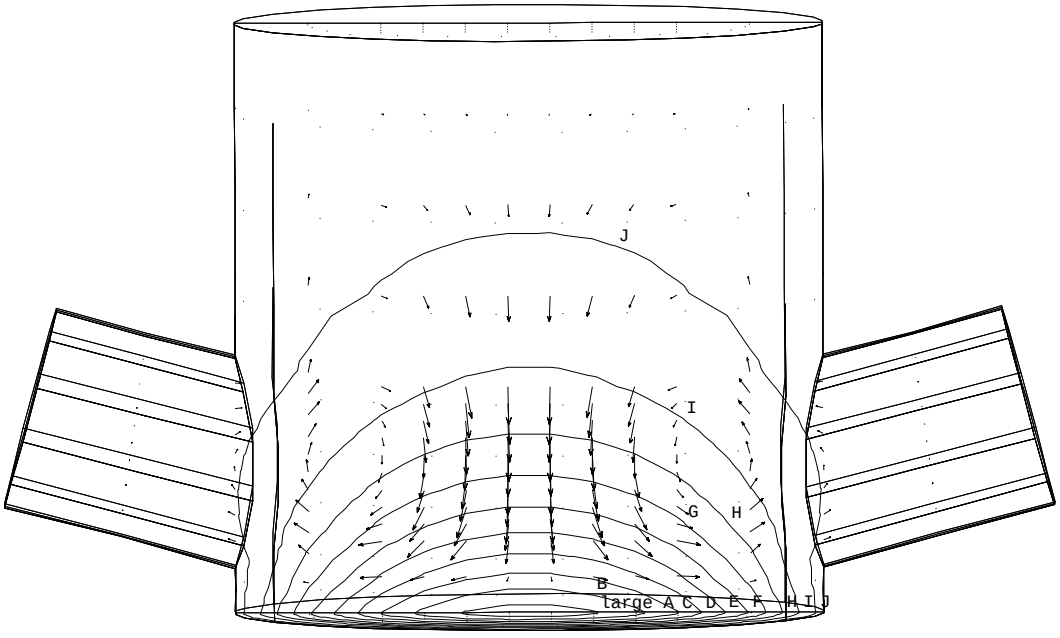

FIG. 5. *Velocity vectors and isotherms at* 10^{-2} *Earth gravity*

TABLE 2
Temperature legend for isotherms

Isotherm	Temperature, ^{o}K
A	1294
B	1295
C	1297
D	1298
E	1300
F	1301
G	1303
H	1304
I	1306
J	1307

TABLE 3
Speed of Simulated Flows

Gravity	Speed m/sec
$1\mathbf{g}$	$.383 \times 10^{-2}$
$10^{-1}\mathbf{g}$	$.890 \times 10^{-3}$
$10^{-2}\mathbf{g}$	1.01×10^{-4}
$10^{-4}\mathbf{g}$	1.05×10^{-6}
$10^{-6}\mathbf{g}$	1.05×10^{-8}

To examine whether the flows might have significant temporal fluctuations, we turn to the Rayleigh number

$$Ra = \frac{\rho^2 c_p \mathbf{g} \beta L \Delta T}{\kappa \mu},$$

where β is from Eqn. (2), the temperature difference is $\Delta T = 15$, and ρ_0 is taken from Table 1. Direct simulations of two-dimensional buoyancy driven flows indicates that stable flow conditions exist for $Ra < 9.0 \times 10^3$ [17], and that the transition to turbulence would take place for Rayleigh numbers in the range 10^5 to 10^7 [13]. The Earth-gravity calculations presented here has a value of the Rayleigh number $Ra_{earth} \approx 1300$. Since this value decreases as we move to reduced gravity conditions, we expect that the experiment would have stable flow conditions with negligible temporal fluctuations in the absences of disturbances in the acceleration forces due to gravity.

The absence of gravity fluctuations may not be a good assumption. For example, astronaut activities and firing of booster rockets can have effects of $10^{-6}\mathbf{g}$ to $10^{-2}\mathbf{g}$ aboard the space shuttle [18]. Thus, we examine the differences in the temperature profiles of the simulations under various orientations, with the

results in Table 4. Here, T_{ref} is the temperature from the simulation at $10^{-2}\mathbf{g}$

TABLE 4
Temperature variations

Gravity Magnitude	θ (degrees)	ϕ (degrees)	$\|\|T - T_{ref}\|\|_\infty$
$10^{-2}\mathbf{g}$	0	180	.1127
$10^{-2}\mathbf{g}$	0	90	.1364
$10^{-2}\mathbf{g}$	90	90	.1004
$1\mathbf{g}$	0	0	2.397
$10^{-1}\mathbf{g}$	0	0	.5055
$10^{-4}\mathbf{g}$	0	0	.1127
$10^{-6}\mathbf{g}$	0	0	.1083

(see Fig. 5), and we compute the maximum difference (pointwise) between the temperatures in our simulations. The values of θ and ϕ are the rotation of the gravity vector with respect to the plane in which the small tubes are positioned and with respect to the axis of large tube respectively. Thus, $(\theta, \phi) = (0, 0)$ is the original orientation, and $(\theta, \phi) = (0, 180)$ is upside-down, and $(\theta, \phi) = (0, 90)$ has the gravity vector in the same plane as Fig. 5 pointing to the right. When weighting the temperature differences by $1/\Delta T = 1/15$, it can be seen that once the gravity is at $10^{-2}\mathbf{g}$ or lower, the orientation of the ampoule effects temporal gradients less than 1%, but that the comparison of $10^{-2}\mathbf{g}$ with $10^{-1}\mathbf{g}$ and $1\mathbf{g}$ show variations of 3% and 16%, respectively.

Thus, the data in Table 4 indicate that heat transport is dominated by conduction. Another method to discover the dominant force effecting heat transport is by scale analysis. Here, we follow the analysis of [18] to determine the largest magnitude of the acceleration forces required to obtain a thermal boundary-layer thickness the entire length of the ampoule. The reasoning is that if the thickness of the layer, as predicted by the scale analysis, is the entire ampoule, then heat transport will be conduction driven since the heat sources are assumed to be entirely from the boundary conditions on the walls of the ampoule. Since our Prandtl number $Pr = c_p\mu/\kappa \approx .728$ which is less than unity, we need to reduce the acceleration forces (gravity) to $\mathbf{g}_0$ until $PrRa_0 = 1$. Thus, the experiment should be run with acceleration forces $\mathbf{g}_0 \leq 1/PrRa_{earth}$, or at about $10^{-3}\mathbf{g}$. This confirms our transition to conduction-driven heat transport at $10^{-2}\mathbf{g}$.

Effect on Beam Angle

Given the above data from simulations, the question remains as to what effect the density variations have on the angle of the laser beam. We approximate this

effect using Snell's law of refraction [19]

$$n_1 \sin\theta_1 = n_2 sin\theta_2 \tag{5}$$

for light entering a medium with different density, where the refractive index is given by the Dale-Gladstone law $n_i = h\rho_i + 1$, and θ_i is the angle the light makes with the normal vector of the interface between the mediums. Here, $h = 2.26 \times 10^{-4} m^3/kg$ is the Dale-Gladstone constant. The density is computed using the perfect gas law holding pressure constant at $P = 3.42 \times 10^5$ Pascals. We subdivide the laser beam path into 27 equi-distant points p_i, where p_0 is the point where the beam enters the ampoule, and p_{26} is the location along the center axis of the large ampoule where the beam contacts the substrate. Temperature data is interpolated at these 27 points and at points along a path parallel to the laser beam approximately a distance $p_1 - p_0$ from the laser beam, and our calculations are based on this data. Along the beam path, we treat the density as being piecewise constant between points. At each point p_i, the beam bends according to Eqn. (5), where the density is computed using Eqn. (4) based on the interpolated temperature data. The normal to the isotherm at each point is

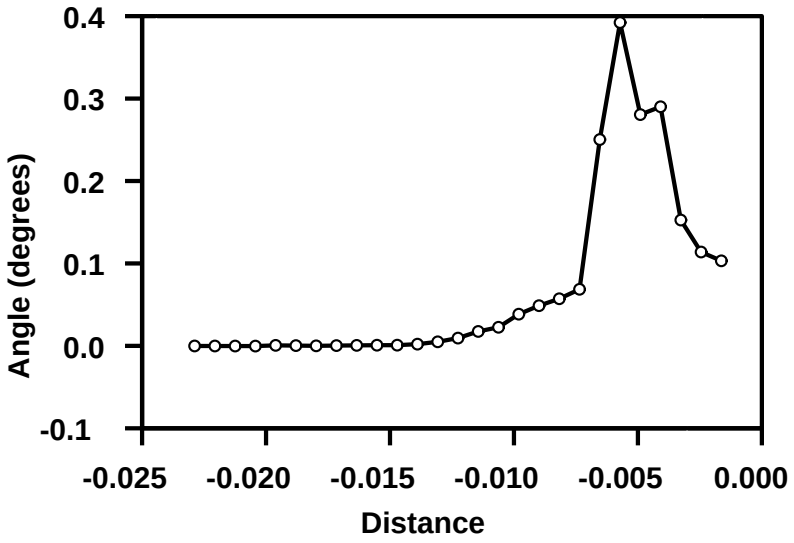

FIG. 6. *Incremental change in beam angle using Snell's Law*

approximated to first order computed using the interpolated temperature profile. The results are summarized in Figs. 6 and 7. We remark that improvements to these calculations are likely to result by replacing Eqn. (5) with a better model for the effects of density variations on the direction of the laser bending, or by using higher-order numerical approximations to the normal direction at each point. Even given the low accuracy of these calculations, the indication is

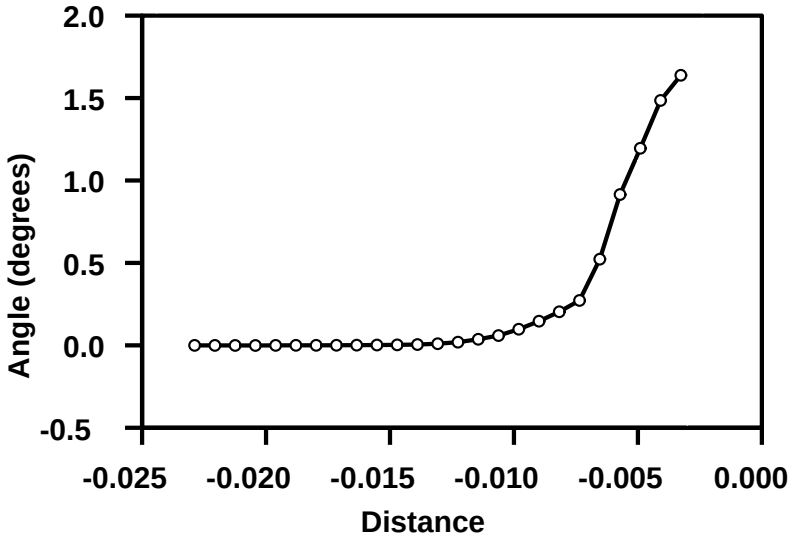

FIG. 7. *Total change in beam angle using Snell's Law*

that laser beam bending due to density fluctuations are likely, and should be studied. We remark that lenses outside the ampoule that focus/defocus might be effective in correcting for density fluctuation effects [20].

Concluding remarks

In this paper, fluid dynamics in a vertical reactor for high pressure vapor transport is discussed. The numerical modeling of thermo-solutal convection shows the effects of gravitational acceleration on temporal gradients near earth condition and in microgravity environment. Orientation of the reactor with respect to the gravity vector and low gravity has little effect on the temperature variations. However, calculations for near earth conditions ($> 10^{-2}\mathbf{g}$) show a stronger impact of gravity on the temperature variations. There is good agreement of the conclusions from the simulations with scale analysis that predicts the onset of conduction-driven thermal transport. The results from the calculations of incidence and refraction angle for a wave undergoing reversible refraction between isotropic media using Snell's law of refraction suggest the potential for significant effects of density/temperature variations on the beam bending.

Our simplified 3D model presented in this paper needs further enhancements for modeling growth at high pressure. The refinements to be included in future studies will include gas-phase chemical reactions, multiple species, thermal (Soret) diffusion, the study of compressibility, and transient calculations.

REFERENCES

[1] S. Ostrach. Low-gravity fluid flows. *Ann. Rev. Fluid Mech.*, 14:313–345, 1982.

[2] N. Dietz, A. Miller, and K.J. Bachmann. Real time monitoring of homoepitaxial and heteroepitaxial processes by p-polarized reflectance spectroscopy. *J. Vac. Sci. Technol.*, A13:153–155, 1995.

[3] N. Dietz and H.J. Lewerenz. An optical in-situ method for layer growth characterization. *Applied Surface Science*, 69:350–354, 1993.

[4] H.K. Moffat and K.F. Jensen. Three-dimensional flow effects in Silicon CVD in horizontal reactors. *J. Electrochemical Society*, 135:459–471, 1988.

[5] S.A. Gokoglu, M. Kuczmarski, P. Tsui, and A. Chait. Convection and chemistry effects in CVD - A 3-D analysis for Silicon deposition. *J. De Physique*, 50:17–34, 1989.

[6] J. Ouazzani and F. Rosenberger. Three-dimensional modeling of horizontal chemical vapor deposition I. MOCVD at atmospheric pressure. *J. Crystal Growth*, 100:545–576, 1990.

[7] Jalil Ouazzani, Kuan-Cheng Chiu, and Franz Rosenberger. On the 2d modelling of horizontal cvd reactors and its limitations. *J. of Crystal Growth*, 91:497–508, 1988.

[8] Jalil Ouazzani and Franz Rosenberger. three-dimensional modeling of horizontal chemical vapor deposition. I MOCVD at atmospheric pressure. *J. of Crystal Growth*, 100:545–576, 1990.

[9] H.T. Banks, K. Ito, J.S. Scroggs, H.T. Tran, K.J. Bachmann, H. Castleberry, and S. Fiechter. Gasdynamics and transport in a high-pressure reactor under microgravity conditions. In *Proceedings of the 2nd IEEE Mediteranean Symposium on New Directions in Control and Automation*, pages 427–433. IEEE, June 1994.

[10] K.J. Bachmann, G.-C. Xing, J.S. Scroggs, H.T. Tran, K. Ito, H. Castleberry, and G. Wood. Heteroepitaxy of wide bandgap ternary semiconductors. *Japanese Journal of Applied Physics*, 32:133–138, 1993.

[11] K. Ito, J.S. Scroggs, and H.T. Tran. Mathematical issues in optimal design of a vapor transport reactor. In *Flow Control*, M.D. Gunzburger, editor, pages 197–218, to appear. IMA, 1995.

[12] K. Ito, J.S. Scroggs, and H.T. Tran. Optimal control of thermally coupled Navier-Stokes equations. *SIAM J. Opt.*, submitted.

[13] M.T. Landahl and E. Mollo-Christensen. *Turbulence and random processes in fluid mechanics*. Cambridge University Press, New York, 1992.

[14] S. Fiechter, R.H. Castleberry, G. Wood, K.J. Bachmann, H.T. Tran, K. Ito, and J.S. Scroggs. High pressure vapor transport of binary and ternary compound semiconductors. In *Proceedings of the Sixth International Symposium on Experimental Methods for Microgravity Materials Science*, page to appear. TMS, 1994.

[15] G. Eriksson and K. Hack. Chemsage–a computer program for the calculation of complex chemical equilibria. *Metallurgical Transactions B*, 21B, 1990.

[16] Roger A. Svehla. Estimated viscosities and thermal conductivities of gases at high temperatures. Technical Report NASA TR R-132, NASA, Washington, D.C., 1962.

[17] W.M.B. Duval. Transition to chaos in the physical vapor transport process – I. In *Fluid Mechanics Phenomena in Microgravity, 1993*, pages 51–64, New York, November 1993. ASME.

[18] N. Ramachandran, C.R. Baugher, and M.J. Rogers. Acceleration environment on the space shuttle and its impact on thermo-solutal fluid mechanics. In *Fluid Mechanics Phenomena in Microgravity, ASME 1993*, pages 155–171, New York, November 1993. ASME.

[19] J.R. Meyer-Arendt. *Introduction to Classical and Modern Optics*. Prentice-Hall, New Jersey, 1984.

[20] J.E. Smith. personal communcations, February, 1995.